Available online at www.sciencedirect.com

SciVerse ScienceDirect

Ceramics International 39 (2013) 6019–6028

CERAMICS INTERNATIONAL

www.elsevier.com/locate/ceramint

# Effects of $Cr_3C_2$ addition on the erosion–corrosion behavior of Ti(C,N)-based cermets

Weicai Wan, Ji Xiong*, Zhixing Guo, Guangbiao Dong, Chenghong Yi

*School of Manufacturing Science and Engineering, Sichuan University, Chengdu 610065, PR China*

Received 13 November 2012; received in revised form 6 January 2013; accepted 8 January 2013
Available online 16 January 2013

**Abstract**

The effect of $Cr_3C_2$ addition on the erosion–corrosion behavior of Ti(C,N)-based cermets was investigated. The results indicate that the erosion–corrosion resistance of cermets is significantly enhanced by $Cr_3C_2$ addition due to corrosion resistance and mechanical property improvement. Strengthening of Ni binder phase by Cr atoms dissolution also contributes to the improvement in erosion–corrosion resistance of cermets. With the increase of $Cr_3C_2$ content, the erosion–corrosion behavior of cermets is classified to corrosion regime, erosion affected corrosion regime, corrosion affected erosion regime and erosion regime. The corrosion resistance of binder plays an important role in the erosion–corrosion degradation of cermets. Erosion damage is covered by severe corrosion of binder phase for the cermets with low $Cr_3C_2$ addition, while for the cermets containing high $Cr_3C_2$ content, the material deterioration is governed by the mechanical impingement of solid erodents.


*Keywords:* C. Corrosion; C. Wear resistance; D. Ti(C,N)-based cermets

## 1. Introduction

In recent years, Ti(C, N)-based cermets have been successfully introduced into the metal cutting industry and other wear resistance operations as an alternative to WC–Co cemented carbides because of the relatively low production cost and excellent properties such as high heat-hardness, perfect chemical stability, low friction coefficient, and superior thermal deformation resistance [1–4].

The erosion–corrosion degradation widely occurs in the petroleum production and refinery, chemical engineering, coal and hydropower industries [5–7], and this behavior involves the corrosion damage caused by corrosive medium and the mechanical wear failure due to the erosion of solid particles and liquids. Corrosion and mechanical erosion may interact synergistically to cause wear rate that is greater than the sum of their separate effects [8–13]. In such aggressive circumstances, the knowledge of pure corrosion resistance or wear resistance is insufficient to enable cost-effective selection of an appropriate material for the erosion–corrosion service [5]. Up to now, limited information on the erosion–corrosion performance of metal–ceramic composites is available. The degradation mechanism of WC-based cermets was researched by M. Reyes and A. Neville for drilling tools offshore [6], and they believed that erosion models, which were useful and valid in dry erosion, had some limitations in liquid–solid impingement conditions due to the increased complexity of particle trajectories and the effect of corrosion. N. Espallargas et al. [7] pointed out that the relative importance of erosion and corrosion should be considered when a material was selected for the operation of erosion–corrosion resistance. E.J. Wentzel and C. Allen [8,9] investigated the erosion–corrosion resistance of hard metals with different binder compositions. They found that the differences in binder composition influenced the cermets' mechanical properties and corrosion behavior, which in turn affected the synergistic action of erosion and corrosion. They further noticed that the main mechanism of material loss during slurry erosion was binder removal,

*Corresponding author. Tel.: +86 13880085119; fax: +86 28 85196764.
*E-mail addresses:* hardmetal313@yahoo.com.cn, wj927vick@sina.com (J. Xiong).

0272-8842/$ - see front matter © 2013 Elsevier Ltd and Techna Group S.r.l. All rights reserved.
http://dx.doi.org/10.1016/j.ceramint.2013.01.016

followed by WC grain detachment. In addition, A. Neville et al. [11] studied the erosion–corrosion behavior of WC-based metal matrix composites in liquid–solid slurries with different sand particles size and sand loading. The researchers concluded that a little difference in erosion–corrosion rate was recorded for the different WC grain size fractions, and the erodent size was extremely important not only in terms of the total mass loss but the performance of different materials.

It is well accepted that the erosion–corrosion resistance of materials is influenced significantly by mechanical properties and corrosion resistance. On the one hand, the microstructure and mechanical properties of Ti(C,N)-based cermets are affected by $Cr_3C_2$ addition [2–4]. In literatures [4,14–16], it is reported that $Cr_3C_2$ addition inhibits grains growth effectively in cermets. It is known that the hardness of cermets increases with the grains size decreasing in term of a modified Hall–Petch relationship [17]. Hardness is usually accepted to be the best indicator of wear resistance, and materials with higher hardness are usually assumed to be more wear resistant [18]. However, during erosion, materials with harder surface do not always have a higher wear resistance [18–23], because the hard and stiff ceramic skeleton is too brittle to sustain the high local stress, and it is more likely to be broken through intergranular and/or transgranular modes [20]. On the other hand, $Cr_3C_2$ is an effective additive to enhance the corrosion resistance of materials [24–29]. Nevertheless, it should be noted that the excellent passivation behavior of materials may well negate the superior corrosion resistance under conditions where any passive film is continuously removed, such as in slurry erosion [8,9]. Consequently, the relationship between erosion–corrosion resistance and any single property is far from straightforward. The mechanical property and corrosion resistance of Ti(C,N)-based cermets are expected to be improved with $Cr_3C_2$ addition, thus it is necessary for $Cr_3C_2$ addition to remarkably influence the erosion–corrosion behavior. Accordingly, it is of vital importance to study the effects of $Cr_3C_2$ addition on the erosion–corrosion behavior of cermets.

In the work, the erosion–corrosion behavior of Ti(C,N)-based cermets with different $Cr_3C_2$ content is investigated using a home-made experimental device. In order to simulate the harsh environments, a slurry of sulfuric acid solution and alumina sands is used as the flowing medium, since sulfuric acid is the typical aggressive environments in industries and $Al_2O_3$ sands can cause a serious destruction on the surface of target materials owing to the high hardness. The main purpose of this paper is to investigate the influence of $Cr_3C_2$ addition on the erosion–corrosion performance of cermets.

## 2. Experimental procedures

### 2.1. Materials and characterization

The characteristics of starting powders used in the work are listed in Table 1. A typical powder metallurgical technique was utilized to produce four grades of experimental materials. The compositions of cermets are given in Table 2. The powders mixture was ball-milled in stainless steel lined mills using WC-8 wt.% Co balls with a diameter of 10 mm as milling bodies for 72 h, using alcohol as the milling medium, and the milling speed was 68 rpm. The balls to powders weight ratio was fixed at 10:1. After the powders were pressed to green bodies, the compact specimens were sintered at 1440 °C for 1 h, with the vacuum degree of 5 Pa.

The microstructures of samples were evaluated using an S-4800 scanning electron microscope (SEM; Hitachi Company, Japan) in backscattered electrons mode (BSE). The micro-morphology of cermets is shown in Fig. 1. The cermets have the typical core/rim microstructure. The dark undissolved Ti(C,N) cores are surrounded by a grayish rim, and the brighter phase is metal binder in the morphology. The density measurements were performed at room temperature(25 °C) by the Archimedes method. Subsequently, rockwell hardness (HRA) and the transverse rapture strength (TRS) were measured on an ARK-600 Rockwell hardness tester (Akashi, Japan) and a WE-100B universal material testing machine (Changchun testing machine plant, China), respectively. Five separate hardness and TRS measurements were taken for each grade material and results were averaged. The properties characteristics of cermets are tabulated in Table 3.

Table 2
Compositions of the cermets investigated in the study (wt%) [29].

| Cermets | $TiC_{0.7}N_{0.3}$ | $Mo_2C$ | $Cr_3C_2$ | Ni |
|---|---|---|---|---|
| G0 | Balance | 10 | 0 | 15 |
| G1 | Balance | 10 | 1 | 15 |
| G2 | Balance | 10 | 3 | 15 |
| G3 | Balance | 10 | 5 | 15 |

Table 1
Characteristics of starting powders [29].

| Powders | FSSS (μm) | Total carbon (wt%) | Free carbon (wt%) | Oxygen (wt%) | Manufacturer |
|---|---|---|---|---|---|
| $TiC_{0.7}N_{0.3}$ | 1.85 | 13.52 | 0.08 | 0.30 | Changsha Wing Hing High-Tech New Materials Co., Ltd., China |
| $Mo_2C$ | 1.55 | 6.03 | 0.20 | 0.52 | Changsha Wing Hing High-Tech New Materials Co., Ltd., China |
| $Cr_3C_2$ | 1.42 | 13.08 | 0.25 | 0.59 | Changsha Wing Hing High-Tech New Materials Co., Ltd., China |
| Ni | 2.65 | 0.10 | – | 0.10 | Chengdu Nuclear 857 New Materials Co., Ltd., China |

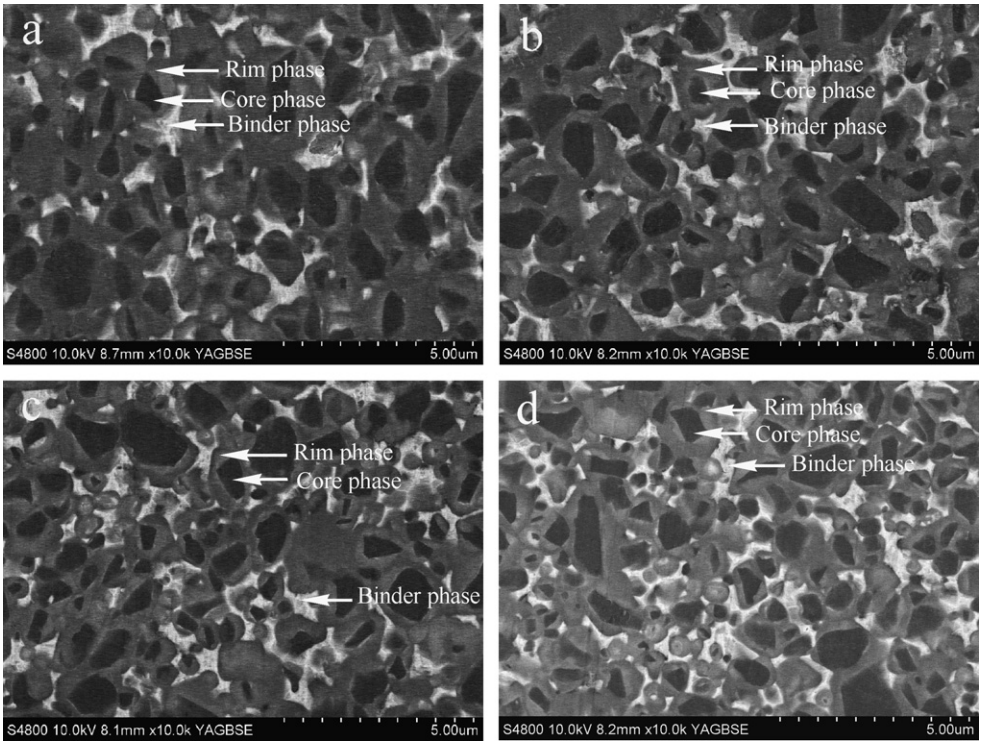


Fig. 1. SEM-BSE micrographs of Ti(C,N)-based cermets with different $Cr_3C_2$ addition [29]: (a) G0:0 wt% $Cr_3C_2$; (b) G1:1 wt% $Cr_3C_2$; (c) G2:3 wt% $Cr_3C_2$ and (d) G3:5 wt% $Cr_3C_2$.

Table 3
Properties characteristics of the cermets.

| Cermets | Relative density (%) | Low magnification microstructure | Hardness (HRA) | TRS (MPa) | Mean grain size(μm) |
|---|---|---|---|---|---|
| **G0** | 99.8 | A02B00C00 | 92.6 | 1300 | 1.58 |
| **G1** | 99.7 | A02B00C00 | 92.6 | 1340 | 1.36 |
| **G2** | 99.8 | A02B00C00 | 92.7 | 1380 | 1.16 |
| **G3** | 99.7 | A02B00C00 | 93.2 | 1430 | 0.81 |

### 2.2. Erosion–corrosion tests

A schematic representation of the erosion–corrosion test apparatus in this work is shown in Fig. 2. Erosion–corrosion tests were carried out using slurry of $Al_2O_3$ sands (150–250 μm) and 0.5 mol/L sulfuric acid solution. $Al_2O_3$ erodent concentration was set at 5wt.%. During the tests, the stainless steel container was filled with 30 L sands/water slurry. The impellers were driven by a motor to prevent sand settling out in the container, and the rotation speed was 550 rpm (the velocity of specimens is 5.76 m/s). Fours stator blades were used in the container. Although the alumina sand erodent was found not to degrade during erosion tests, new erodent was used for each grade specimens.

Four samples of each grade cermet with dimensions of 5 mm × 5 mm × 2 mm were surface ground and polished to 1 μm surface finish using diamond paste. Prior to the erosion–corrosion tests, the initial weight of specimens

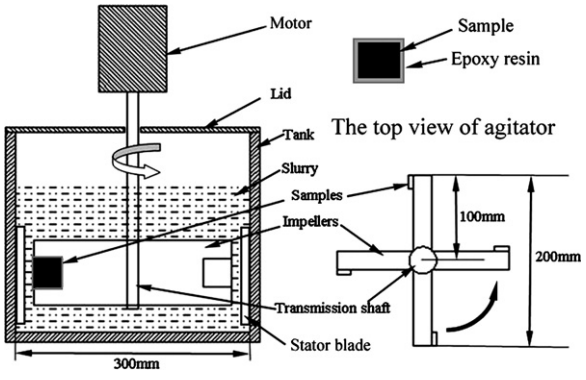


Fig. 2. A schematic representation of the erosion–corrosion test apparatus.

was measured with a precision electron balance model BSA124S (Beijing Sarturius Co., Ltd., China) with the error of 0.1 mg. In order to avoid any edge effect in the

tests, the side faces of the samples were protected by epoxy resin. And then the samples were fixed on the impellers, as shown in Fig. 1. All experiments were performed at room temperature (22–25 °C). The specimens were taken down from impellers every hour, and they were cleaned with acetone using an ultrasonic bath for 5 min in order to remove residual slurry and epoxy resin, and then dried. The weight of each sample was measured for mass loss determination. The test time of each grade material was accumulated to 4 h. The weight loss of each grade material was determined by the average results of four samples. Additionally, static corrosion tests were carried out to assess the effect of corrosion behavior on the erosion–corrosion degradation of cermets. SEM was undertaken on the eroded–corroded surfaces of cermets using secondary electron mode (SE) to examine the morphology, and the chemical compositions on the surfaces were analyzed by energy dispersive spectroscopy (EDS) model OX-FORD IE-250 attached to the SEM.

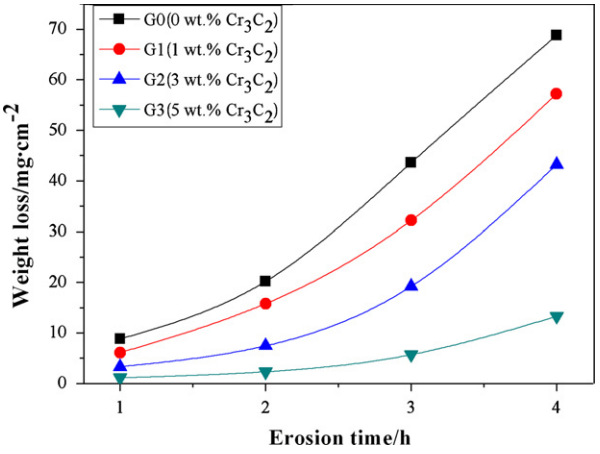


Fig. 3. Weight loss of cermets versus time in erosion–corrosion tests.

## 3. Results

### 3.1. Erosion–corrosion behavior

Fig. 3 shows the weight loss of cermets as a function of test time. It is clear that the weight loss of cermets decreases with the increase of $Cr_3C_2$ content. The weight loss of all cermets increases with the accumulation of time, although this trend is not obvious at the initial stage for cermet G3. It must be noticed that a little difference in material loss is exhibited after all samples suffer to the erosion–corrosion process for 1 h. The material loss of cermets increases drastically in subsequent duration except G3. Particularly, from the figure, it is found that the mass loss of cermet G3 is much lower than the loss of other cermets with time. The relationship between the weight loss and $Cr_3C_2$ addition can be explained by that the mechanical properties and corrosion resistance of materials are influenced by $Cr_3C_2$ addition, resulting in the difference in erosion–corrosion performance.

Fig. 4 shows the attacked surfaces of cermets in erosion–corrosion tests for 2 h. It is evident from the micrographs

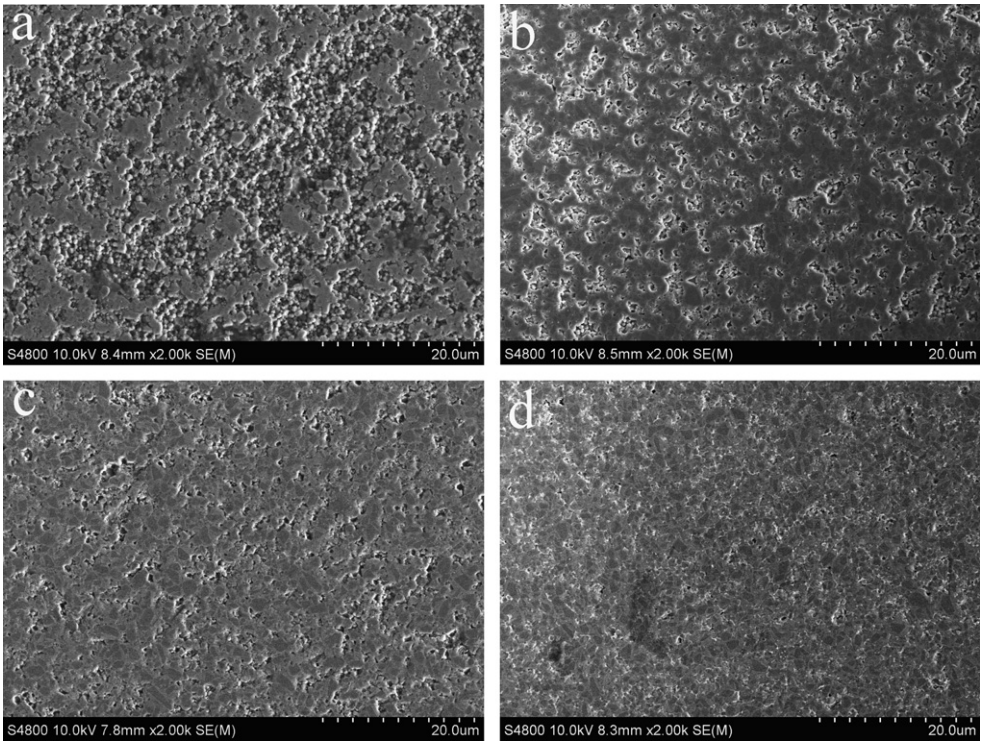


Fig. 4. SEM-SE micrographs of the attacked surface of Ti(C,N)-based cermets subjected to erosion–corrosion process for 2 h: (a) G0:0 wt% $Cr_3C_2$; (b) G1:1 wt% $Cr_3C_2$; (c) G2:3 wt% $Cr_3C_2$ and (d) G3:5 wt% $Cr_3C_2$.

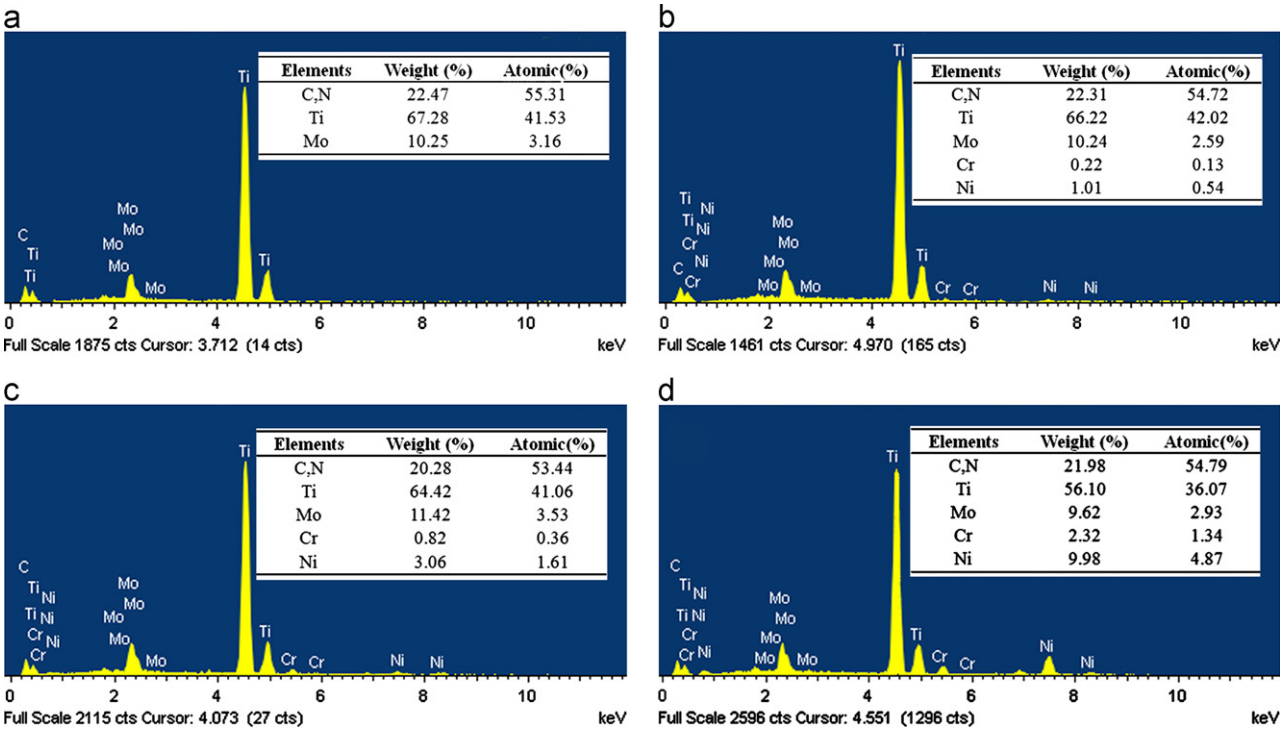


Fig. 5. EDS analysis of the attacked surface of cermets in erosion–corrosion conditions for 2 h: (a) G0:0 wt% $Cr_3C_2$; (b) G1:1 wt% $Cr_3C_2$; (c) G2:3 wt% $Cr_3C_2$ and (d) G3:5 wt% $Cr_3C_2$.

that the damage is alleviated significantly on the surfaces with the increment in $Cr_3C_2$ addition. This observation is consistent with the result of weight loss measurement. EDS analysis of the surfaces is shown in Fig. 5. The result reveals that the variation of Ni content is very obvious on the surfaces of different cermets. Ni is not detected on the surface of cermet G0, and a small amount of Ni is found on the surfaces of cermets G1 and G2. However, in Fig. 5(d), the compositions of attacked surface are similar with the original compositions, and it indicates that the binder loss is insignificant for cermet G3 in the experimental conditions.

Morphologies characteristics of the eroded–corroded surfaces are exhibited clearly in Fig. 6. The degradation is relatively homogeneous in Fig. 6(a). The binder phase is hardly seen, and the grains with planar facets (shown by white arrows) widely scatter on the surface. It is the evidence of the ceramic particles falling off after the metal binder loss. The inhomogeneous morphology is found in Fig. 6(b). On the surface, together with deep erosion pits as a result of ceramic particles pullout, some intact core/rim grains are also observed. In particular, it must be noted that some micro-cracks appear on the surface, as illustrated by arrows. In Fig. 6(c), it is observed that there are many broken ceramic grains with cracks and clear core/rim grains besides erosion pits. Moreover, the evidence of binder corrosion is visible owing to the small pits. Compared to Fig. 6(a,b,c), the damage is relatively slight in Fig. 6(d). The brighter binder phase exists on the surface, and there are only a few small pits. It is therefore believed that cermet G3 has the most superior degradation resistance in the tests.

Fig. 7(a) shows the morphologies of cermet G3 eroded for 4 h. A serious damage is seen on the surface, and residual binder phase and fragments of hard phase are observed clearly. Fig. 7(b) is EDS analysis of the attacked surface. From the result, a high Ni content is detected, and it implies that a preferential binder loss due to corrosion does not occur.

### 3.2. Corrosion behavior

In order to examine the influence of corrosion behavior on the erosion–corrosion degradation, immersion corrosion tests are conducted to correlate the corrosion resistance of cermets with $Cr_3C_2$ content in the corrosive environments. Figs. 8 and 9 are the weight loss and corrosion morphology of cermets immersed in corrosive solution for 2 h, respectively. In Fig. 8, the weight loss of cermets decreases remarkably when an increasing $Cr_3C_2$ content is added into the materials. From Fig. 9(a), lots of deep corrosion pits are observed as a consequence of binder degradation. Corrosion pits in Fig. 9(b,c) are smaller than those in Fig. 9(a). Only a few corrosion pits and relatively intact binder are seen from Fig. 9(d), and it indicates a slight binder corrosion. According to the result of corrosion tests, a general trend of reducing corrosion degradation of binder phase with the increase of $Cr_3C_2$ content is followed for the test materials. Thereby, it is

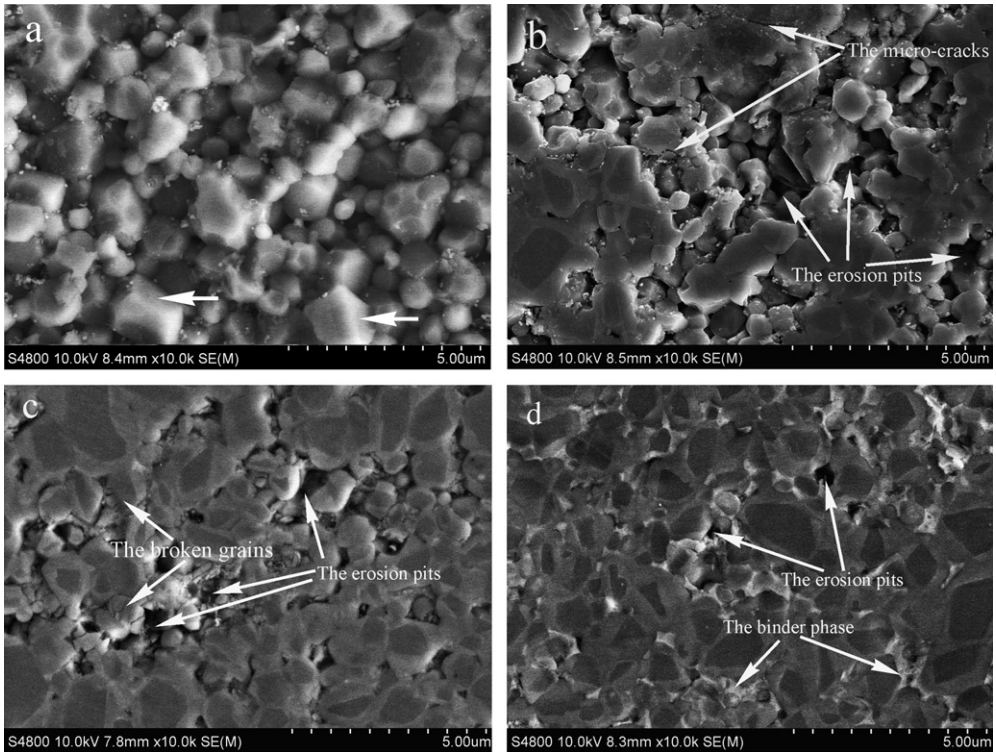


Fig. 6. Localized morphology of the surface of Ti(C,N)-based cermets subjected to erosion–corrosion process for 2 h: (a)G0:0 wt% $Cr_3C_2$; (b) G1:1 wt% $Cr_3C_2$; (c) G2:3 wt% $Cr_3C_2$ and (d) G3:5 wt% $Cr_3C_2$.

evident that the corrosion resistance of Ni binder is strengthened considerably by $Cr_3C_2$ addition.

### 3.3. Classification of erosion–corrosion behavior

In literatures [30–32], the authors classified the erosion–corrosion behavior of materials to four categories: erosion dominated regime, erosion–corrosion dominated regime, corrosion–erosion dominated regime and corrosion dominated regime. The models of classification are referred to in this study.

Corrosion tests indicate that the corrosion behavior of binder phase plays an important role in degradation of cermet G0 under the erosion–corrosion conditions because of the poor corrosion resistance. After the binder phase is etched off in the corrosive liquid, the unsupported ceramic particles fall off from the surface. There is no erosion characteristic such as micro-cracks caused by the impingement of abrasive particles on the surface. It means that the erosion effect of erodent is concealed by the severe corrosion of binder phase. Hence, it is reasonable to believe that the deterioration of this material is defined as corrosion regime. A small quantity of Ni is remained on the attacked surface of cermet G1 by EDS analysis. Fig. 9(b) also shows that adding 1wt% $Cr_3C_2$ into the cermets cannot sufficiently prevent the binder corrosion in the corrosive slurry. Hence, the binder corrosion is still a vital degradation mechanism of the failure of cermet G1 in erosion–corrosion tests. On the other hand, some cracks

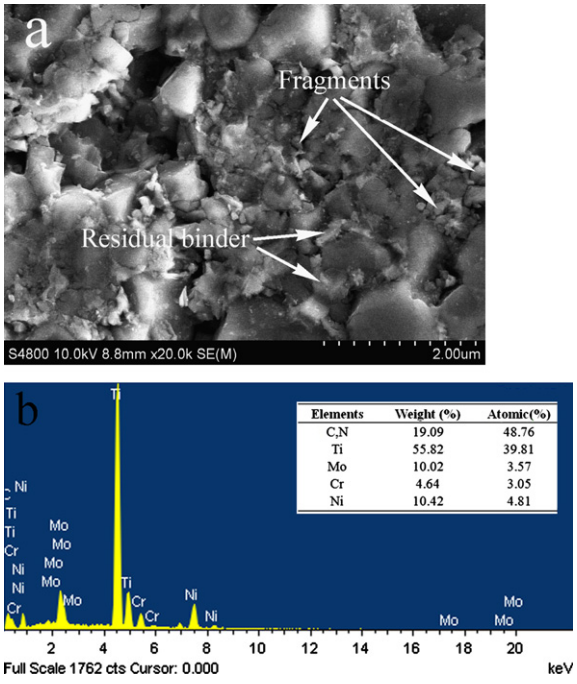


Fig. 7. SEM-SE micrographs and EDS analysis of the surface of cermet G3 (5wt% $Cr_3C_2$ addition) in erosion–corrosion conditions for 4 h: (a) morphology and (b) EDS analysis.

appear on the eroded surface and it is the evidence of erosion destruction. It is believed that the deterioration of cermet G1 is determined by the combination of corrosion

and erosion. Whereas, owing to only a few cracks, the mechanical impact plays a secondary role in the degradation of the cermet. In other words, the degradation behavior of cermet G1 is erosion affected corrosion regime. On the attacked surface of cermet G2, many cracks and crushed ceramic particles are observed and the result of EDS analysis reveals the residual binder phase increasing compared with cermets G0 and G1. According to the morphology observation and EDS result, the deterioration of cermet G2 is controlled by mechanical erosion and corrosion, while erosion prevails. The behavior is considered as corrosion affected erosion regime. With the further improvement in the corrosion resistance, the corrosion of material containing 5 wt% $Cr_3C_2$ is negligible in the slurry due to the relatively intact binder phase, as shown in Figs. 6(d) and 9(d). After the cermet G3 is subjected to the corrosive slurry for 4 h, the preferential binder loss is not still observed. It implies that the failure of materials is determined by the impingement of erodents on the basis of prominent erosion characteristics. Thus, this behavior is defined as erosion regime. In summary, with the increase of $Cr_3C_2$ addition, the classification of the erosion–corrosion behavior of Ti(C,N)-based cermets is illustrated schematically in Fig. 10.

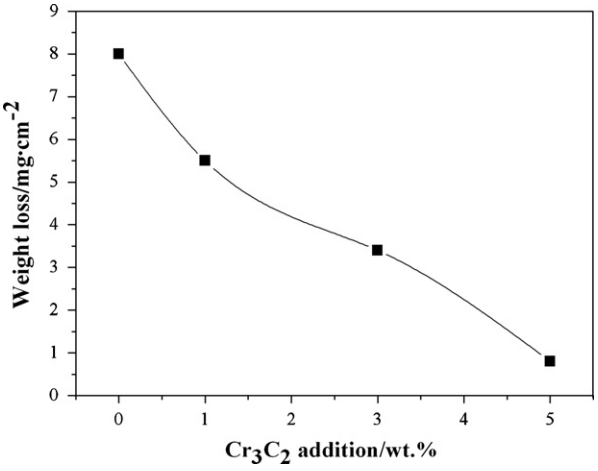


Fig. 8. Weight loss of cermets in corrosion tests.

### 3.4. EDS analysis of binder phase

EDS analysis of binder phase is carried out as shown in Fig. 11. The Cr content in Ni binder phase is tabulated in Table 4. The Cr content in binder phase is raised remarkably with the increase of $Cr_3C_2$ addition.

## 4. Discussion

In corrosion regime, corrosion of binder phase is prevalent. Ni binder phase is corroded off firstly in acidic environments, especially at the interphase between metal binder and ceramic particles [5–7]. The binder corrosion is thought to a precursor of hard phase removal from the surface. The unbonded ceramic particles are easily plucked off under the effect of stirred water and sands [5,7]. In this regime, the impact behavior of solid particles is concealed,

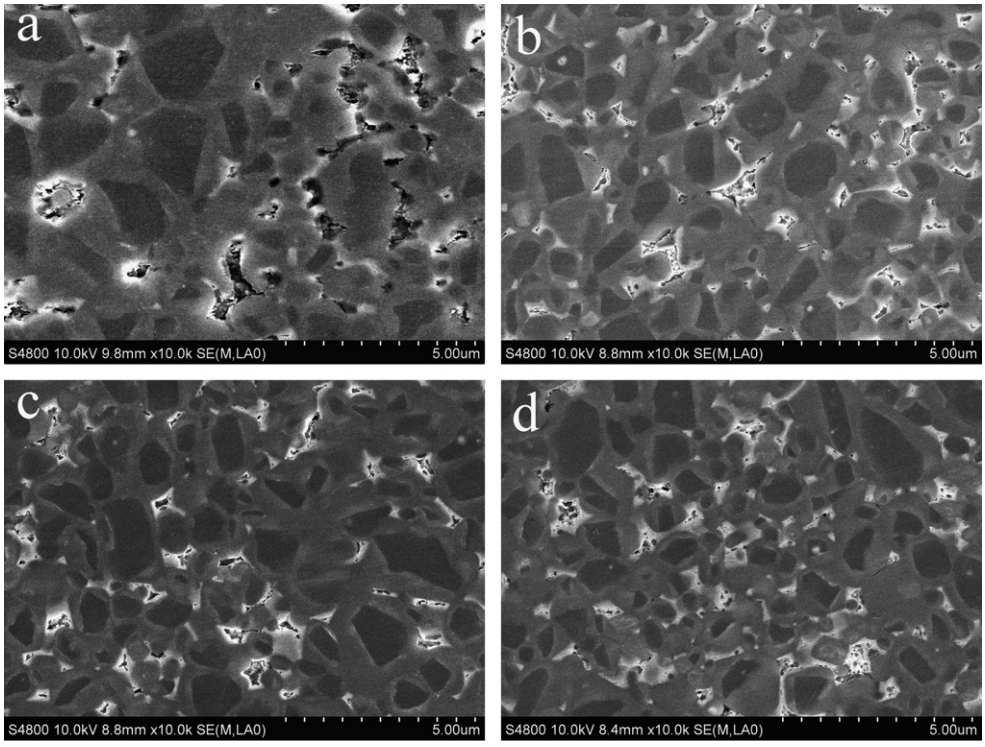


Fig. 9. SEM-SE micrographs of the attacked surface of cermets in corrosion tests for 2 h: (a) G0:0 wt% $Cr_3C_2$; (b) G1:1 wt% $Cr_3C_2$; (c) G2:3 wt% $Cr_3C_2$ and (d) G3:5 wt% $Cr_3C_2$.

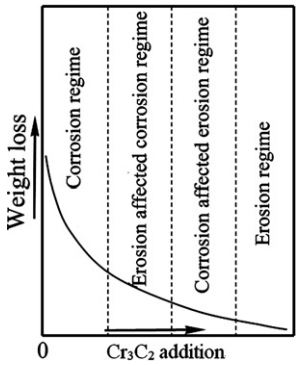


Fig. 10. Schematic of the categories on the erosion–corrosion behavior of Ti(C,N)-based cermets with different $Cr_3C_2$ addition.

but the erosion effect cannot be ignored. In such short test time of 2 h, it is impossible that metal binder phase on the surface dissolves completely into corrosive slurry, although erosion conditions will significantly enhance the rate of metal dissolution due to corrosion [5,6]. The reasonable explanation is that after the interfacial bonding is damaged, the residual binder phase is removed by erosion action of liquid and solid. The erosion failure of cermets starts with transmission of impact energy from the solid erodent to target material during collisions. Collisions result in accumulation of elastic strain energy (fracture energy) and cracks formation at flaws of cermets [7,33]. Energy accumulates with erosion time when other parameters are constant. For the cermets in corrosion regime, before the formation and propagation of cracks on the surface, the ceramic particles have been pulled out from the material due to binder phase loss. Therefore, the erosion features such as cracks and grains fracture are not observed from the damage morphology.

For the cermets in erosion affected corrosion regime, the corrosion resistance of binder phase is improved slightly by a little $Cr_3C_2$ addition. To a certain extent, the protection of binder to ceramic phase is strengthened in the acidic conditions, and then it takes a longer time to pluck out the ceramic particles from the matrix. Thus, before the removal of ceramic particles, it is necessary for the grains to gain higher impact energy. When the absorbed energy of target materials increases to a certain value, the nucleation of cracks occurs at flaws. Thereby, the cracks appear on some grains which are relatively fragile.

In corrosion affected erosion regime, the erosion damage of cermets is highlighted with the further improvement of corrosion resistance. The ceramic particles are expected to accumulate a higher energy leading to cracks propagation and grains fracture before grains pullout occurring, as the aforementioned mechanism. This means that the difficulty in grains pullout promotes erosion appearing, so the erosion characteristics can be exhibited obviously on the surface.

In erosion regime, the corrosion behavior is insignificant in the aggressive environments for the cermets. Static corrosion test demonstrates that the cermet G3 has an excellent corrosion resistance in the corrosive slurry. Erosion attack of $Al_2O_3$ erodent is a decisive factor to material degradation. When hard erodent impinges repeatedly on the cermets, the local plastic flow of binder phase dominates during initial impacts [34], and then the fatigue failure occurs under the continuous impingements of solid particles [7]. Subsequently, the relative fine ceramic particles are squeezed out from Ni metal matrix, because the grain having a larger size confers improved resistance to grains pullout [34]. On the other hand, the nucleation and propagation of cracks occur as a result of the energy accumulation. Finally, the broken grains and fragments are plucked out from the eroded surface.

Apart from the effect of $Cr_3C_2$ on corrosion resistance of binder phase, the alloying of binder phase must be taken into consideration in any discussion of the tribological performance, because the erosion resistance of cermets depends strongly on the alloying of binder [18]. It is reasonable that the Cr content in the binder phase increases with the increase of $Cr_3C_2$ addition. In sintering, the Cr atoms dissolve preferentially in Ni binder, and Cr is a strong solid-solution strengthening element in Ni [29]. The Ni binder phase is strengthened with the increase of $Cr_3C_2$ content in cermets. It is desirable to increase $Cr_3C_2$ addition for the improvement in erosion performance of cermets.

It is accepted that the mechanical properties are of the utmost importance to erosion behavior of materials. Hardness of cermet G3 increases sharply (as shown in Table 3), since the grains are refined remarkably by 5 wt% $Cr_3C_2$ addition. Increase in hardness is found to be advantageous for the improvement in erosion resistance of a brittle material [9,17], although some researchers have pointed out that there is not a log-linear relationship between hardness and materials loss in erosion conditions [6,19]. Furthermore, the fracture strength of grains increases as size decreasing [19], so grains refinement is helpful to restrain the formation and propagation of cracks. Thus, the rise in erosion resistance of cermet G3 is likely to be associated with grains refinement. Namely, the improvement in mechanical property of the cermets with proper $Cr_3C_2$ addition can be attributed to the enhancement of the erosion performance.

## 5. Conclusions

In the study, investigations have been conducted to correlate the erosion–corrosion behavior of Ti(C,N)-based cermets with $Cr_3C_2$ addition. The main findings are concluded as follows.

(1) The erosion–corrosion resistance of Ti(C,N)-based cermets are improved significantly by $Cr_3C_2$ addition in a slurry of 0.5 mol/L $H_2SO_4$ solution and 5 wt% $Al_2O_3$ sands.
(2) The erosion–corrosion degradation of Ti(C,N)-based cermets containing different $Cr_3C_2$ addition is classified to corrosion regime, erosion affected corrosion regime, corrosion affected erosion regime and erosion regime in the testing conditions.

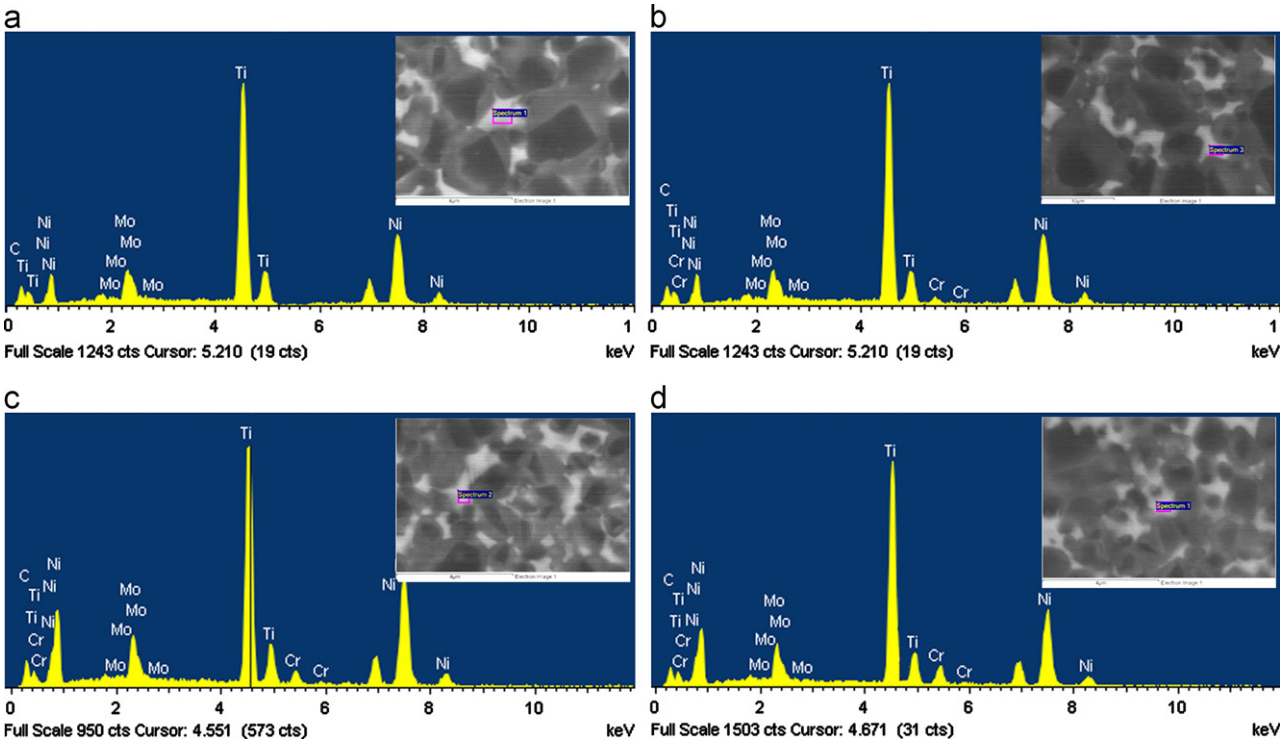


Fig. 11. EDS analysis of binder phase: (a) G0:0 wt% $Cr_3C_2$; (b) G1:1 wt% $Cr_3C_2$; (c) G2:3 wt% $Cr_3C_2$ and (d) G3:5 wt% $Cr_3C_2$.

Table 4
Cr content in the binder phase of cermets (at%).

| **Cermets** | G0 | G1 | G2 | G3 |
|---|---|---|---|---|
| **Cr content** | 0 | 0.80 | 1.34 | 2.53 |

(3) The corrosion resistance of Ni binder is improved remarkably in $H_2SO_4$ environments, and the corrosion property of binder phase plays an important role in the erosion–corrosion behavior of Ti(C,N)-based cermets.
(4) Cr atoms dissolution in metal Ni strengthening the binder phase contributes to the improvement in erosion–corrosion resistance of Ti(C,N)-based cermets.
(5) In erosion–corrosion conditions, the degradation mechanism of cermets with low $Cr_3C_2$ addition is binder phase loss because of corrosion and subsequent detachment of ceramic particles. While for the cermets containing high $Cr_3C_2$ content, the plastic deformation and fatigue damage of binder phase due to the continuous impingement of solid erodent and the debonding and fracture of hard phase are responsible for the material deterioration.

## Acknowledgments

The study is financially supported by National Natural Science Foundation of China (No.51074110) and Chengdu Science and technology Project (no. 10GGZD080GX-268 and 11DXYB096JH-027). Research Funds for the Central Universities (No. 2011SCU11038) and scientist serving enterprise action plan from the Ministry of Science and Technology of China (No. 2009GJF00030). The authors are grateful to Chengdu Mingwu Technology Corp., LTD. of China for supply of materials. Thanks are also extended to Analytical & Testing Center of Sichuan University for the testing of the samples.

## References

[1] P. Ettmayer, H. Kolaska, W. Lengauer, K. Dreyer, Ti(C,N) cermets—metallurgy and properties, International Journal of Refractory Metals and Hard Materials 13 (1995) 343–351.
[2] Y. Zheng, M. You, W.H. Xiong, W.J. Liu, S.X. Wang, Effect of $Cr_3C_2$ on valence-electron structure and plasticity of rim phase in Ti(C,N)-based cermets, Journal of the American Ceramic Society 87 (2004) 460–464.
[3] Y. Zheng, M. You, W.H. Xiong, W.J. Liu, S.X. Wang, Valence-electron structure and properties of main phases in Ti(C,N)-based cermets, Materials Chemistry and Physics 82 (2003) 877–881.
[4] Y. Zheng, W.J. Liu, Q. Yuan, L. Wen, W.H. Xiong, Effect of grain inhibitor on microstructure and mechanical properties of Ti(C,N)-based cermet, Key Engineering Materials 280–283 (2005) 1413–1416.
[5] A. Neville, T. Hodgkiess, Characterisation of high-grade alloy behaviour in severe erosion–corrosion conditions, Wear 233–235 (1999) 596–607.
[6] M. Reyes, A. Neville, Degradation mechanisms of Co-based alloy and WC metal-matrix composites for drilling tools offshore, Wear 255 (2003) 1143–1156.
[7] N. Espallargas, J. Berget, J.M. Guilemany, A.V. Benedetti, P.H. Suegama, $Cr_3C_2$–NiCr and WC–Ni thermal spray coatings as alternatives to hard chromium for erosion–corrosion resistance, Surface and Coatings Technology 202 (2008) 1405–1417.
[8] E.J. Wentzel, C. Allen, The erosion–corrosion resistance of tungsten–carbide hard metals, International Journal of Refractory Metals and Hard Materials 15 (1997) 81–87.

[9] E.J. Wentzel, C. Allen, Erosion–corrosion resistance of tungsten carbide hard metals with different binder compositions, Wear 181–183 (1995) 63–69.
[10] A. Neville, X. Hu, Mechanical and electrochemical interactions during liquid–solid impingement on high-alloy stainless steels, Wear 251 (2001) 1284–1294.
[11] A. Neville, F. Reza, S. Chiovelli, T. Revega, Erosion–corrosion behaviour of WC-based MMCs in liquid–solid slurries, Wear 259 (2005) 181–195.
[12] M.M. Stack, T.M. Abd El Badia, Mapping erosion–corrosion of WC/Co–Cr based composite coatings: particle velocity and applied potential effects, Surface and Coatings Technology 201 (2006) 1335–1347.
[13] T. Hodgkiess, A. Neville, S. Shrestha, Electrochemical and mechanical interactions during erosion–corrosion of a high-velocity oxy-fuel coating and a stainless steel, Wear 233–235 (1999) 623–634.
[14] F.J.J. Kellner, H. Hildebrand, S. Virtanen, Effect of WC grain size on the corrosion behavior of WC–Co based hardmetals in alkaline solutions, International Journal of Refractory Metals and Hard Materials 27 (2009) 806–812.
[15] Y.W. Lei, J. Sun, X.W. Du, Q. Zhai, S.L. Hu, Properties and microstructure of VC/$Cr_3C_2$-doped WC/Co cemented carbides, Rare Metals 26 (2007) 584–590.
[16] S.G. Huang, L. Li, O. Van der Biest, J. Vleugels, VC- and $Cr_3C_2$-doped WC–NbC–Co hardmetals, Journal of Alloys and Compounds 464 (2008) 205–211.
[17] V.A. Pugsley, C. Allen, Microstructure/property relationships in the slurry erosion of tungsten carbide–cobalt, Wear 225–229 (1999) 1017–1024.
[18] I. Hussainova, Effect of microstructure on the erosive wear of titanium carbide–based cermets, Wear 255 (2003) 121–128.
[19] A.J. Gant, M.G. Gee, Structure–property relationships in liquid jet erosion of tungsten carbide hardmetals, International Journal Of Refractory Metals and Hard Materials 27 (2009) 332–343.
[20] M. Antonov, I. Hussainova, Cermets surface transformation under erosive and abrasive wear, Tribology International 43 (2010) 1566–1575.
[21] I. Hussainova, J. Kubarsepp, J. Pirso, Mechanical properties and features of erosion of cermets, Wear 250 (2001) 818–825.
[22] I. Hussainova, Some aspects of solid particle erosion of cermets, Tribology International 34 (2001) 89–93.
[23] H. Reshetnyak, J. Kuybarsepp, Mechanical properties of hard metals and their erosive wear resistance, Wear 177 (1994) 185–193.
[24] W.J. Tomlinson, N.J. Ayerst, Anodic polarization and corrosion of WC–Co hardmetals containing small amounts of $Cr_3C_2$ and/or VC, Journal of Materials Science 24 (1989) 2348–2352.
[25] D. Banerjee, G.K. Lai, G.S. Upadhyaya, Effect of binder-phase modification and $Cr_3C_2$ addition on properties of WC-10Co cemented carbide, Journal of Materials Engineering And Performance 4 (1995) 563–572.
[26] S. Sutthiruangwong, G. Mori, R. Kösters, Passivity and pseudopassivity of cemented carbides, International Journal of Refractory Metals and Hard Materials 23 (2005) 129–136.
[27] B. Bozzini, G.P. De Gaudenzi, M. Serra, A. Fanigliulo, F. Bogani, Corrosion behavior of WC–Co based hardmetal in neutral chloride and acid sulphate media, Materials and Corrosion 53 (2002) 328–334.
[28] G. Mori, H. Zitter, A. Lackner, M. Schretter, Influencing the corrosion resistance of cemented carbides by addition of $Cr_3C_2$, TiC and TaC, in: G. Kneringer, P. Rödhammer, H. Wildner (Eds.), 15th International Plansee Seminar, vol. 2, Plansee Holding AG, Reutte, 2001, pp. 222–236.
[29] W.C. Wan, J. Xiong, M. Yang, Z.X. Guo, G.B. Dong, C.H. Yi, Effects of $Cr_3C_2$ addition on the corrosion behavior of Ti(C, N)-based cermets, International Journal of Refractory Metals and Hard Materials 31 (2012) 179–186.
[30] M.M. Stack, S.M. Abdelrahman, A CFD model of particle concentration effects on erosion–corrosion of Fe in aqueous conditions, Wear 273 (2011) 38–42.
[31] M.M. Stack, N. Corlett, S. Zhou, A methodology for the construction of the erosion–corrosion map in aqueous environments, Wear 203–204 (1997) 474–488.
[32] M.M. Stack, S.M. Abdelrahman, B.D. Jana, A new methodology for modelling erosion–corrosion regimes on real surfaces: gliding down the galvanic series for a range of metal-corrosion systems, Wear 268 (2010) 533–542.
[33] J. Kübarsepp, H. Klaasen, J. Pirso, Behavior of TiC-base cermets in different wear conditions, Wear 249 (2001) 229–234.
[34] B.V. Manoj Kumar, Bikramjit Basu, S. Kang, J. Ramkumar, Erosion wear behavior of TiCN–Ni cermets containing secondary carbides (WC/NbC/TaC), Journal of the American Ceramic Society 89 (2006) 3827–3831.